Int. J. Electrochem. Sci., 13 **(2018)** 2577 – 2584, doi: 10.20964/2018.03.65

International Journal of
ELECTROCHEMICAL
SCIENCE
www.electrochemsci.org

Short Communication

Weld corrosion of GH3535 in molten (Li,Na,K)F

Yanli Wang[1],*Shenghua Zhang*[2,*], *Chaoliu Zeng*[2], *and Weihua Li*[3,*]

[1] School of Chemistry and Chemical Engineering, Guangxi University, Nanning, 530004, P R China.
[2] School of Resources, Environment and Materials, Guangxi University, Nanning, 530004, P R China.
[3] Institute of Metal Research, Chinese Academy of Sciences, Shenyang, 110016, P R China.
[*]E-mail: wyl15104008565@126.com

Received: 14 November 2017 / *Accepted:* 11 January 2018 / *Published:* 5 February 2018

The corrosion of structural materials in molten fluoride salts restricts the development of a molten salt reactor (MSR), with local galvanic corrosion of the weld joint being one of the major failure modes associated with the structural materials in the operating environment of an MSR. In this paper, in situ electrochemical measurements, combined with scanning electron microscopy (SEM/EDX) and metallographic microscope testing methods, are used to study the weld corrosion of GH3535 at 700 ^{o}C in molten (Li,Na,K)F. The results show that each part of the welding areas is in active dissolution state at the open circuit potential. The electrochemical behavior of the heat affected zone is similar to that of the GH3535 parent material. When the weld zone of the GH3535 is coupled with the parent alloy, galvanic corrosion occurs and the galvanic corrosion effect is larger than 1.

Keywords: weld corrosion, GH3535, molten (Li,Na,K)F.

1. INTRODUCTION

A molten salt reactor (MSR) is the only liquid-fueled reactor of the six candidates considered for the Generation IV advanced nuclear reactor, which are characterized by many remarkable advantages, including a unique safety characteristics not found in solid-fuel reactors, economics, no radiation damage constraints on the attainable fuel burn-up, no spent nuclear fuel and so on [1, 2]. Molten fluoride salts are good candidates as the primary reactor coolant, liquid fuel and solvent for MSR systems due to their good thermal conductivity, large specific heat, low viscosity, low vapor pressure at operating temperatures, low melting point, high boiling point and relatively good chemical inertness [3-10]. However, the corrosion of material in molten fluorides at high temperatures, which mainly via the selective dissolution of alloying elements, is an inevitable problem for the application

and development of MSR. In addition, unlike conventional high temperature corrosion [11-13], most metal oxides are chemically unstable in molten fluorides and generally converted to their corresponding metal fluorides. Over the past 60 years, many studies on the corrosion behavior of pure metals and materials in molten fluorides have been conducted by many research institutions, such as ORNL, NASA, the University of Wisconsin, the Chinese Academy of Sciences, and the National Institute for Fusion Science (NIFS) [9-15]. The results of these studies have found that the corrosion resistance of metals increased in the following order: Mo>Ni>Co>Fe>Cr>Ti>Al. The corrosion of Ni-based alloys has been shown to be more serious as the Cr content increases. Finally, the basic principles of alloy designing have been formed, among which the Hastelloy-N (Ni-17%Mo-7%Cr-5%Fe, in terms of mass percent) developed by ORNL exhibits a great potential for long-term applications in corrosive environments [16,17].

The design considerations for an MSR system may involve the use of several different materials which may exhibit different electromotive potentials, and making them susceptible to galvanic corrosion. A galvanic ranking has been identified for most metals in water and seawater systems. Unfortunately, similar rankings have not been developed for various metals in molten fluoride salt systems. Galvanic corrosion is an important corrosion mechanism and a great challenge in molten fluorides in MSR where protective scales are not expected to form on any alloy surfaces [9, 17]. In a study of the compatibility of container materials with Cr in molten FLiNaK salt, Qiu observed that the container materials, graphite and Ni, accelerated the corrosion process between the metallic Cr and the crucibles [18]. This result is mainly ascribed to the different electromotive potentials between metal Cr and the container materials. Wang [9] investigated the galvanic corrosion behavior of pure Ni, Fe, and Cr in molten (Li,Na,K)F at 700 ^{o}C. Galvanic corrosion of the Ni-Cr, Fe-Cr and Ni-Fe couples occurred in the molten (Li,Na,K)F, with the largest galvanic corrosion effect observed for the Ni-Cr couple.

Galvanic corrosion usually occurs as a macroscopic process when macroscopic components of dissimilar metals in contact with an electrolyte. It can also occur microscopically in material with a nominally uniform composition. It is possible to have such an effect at the microstructural level in a welded joint where the weld zone (WZ), heat affected zone (HAZ) and parent material (PM) experience phase changes due to re-precipitation and grain growth, causing them to possess different electrochemical potentials [18]. From a large number of studies, in many corrosion environments, the scrapping of the entire setup happened in advance is mainly due to the preferential corrosion of the welded areas. Therefore, it is very important to study the the galvanic corrosion behavior of the welded joints in an MSR environment. However, up to now, there have been few reports on this topic.

In the present study, the weld corrosion of GH3535 in molten (Li,Na,K)F was investigated in an attempt to garner an in depth understand the corrosion mechanism of galvanic corrosion.

2. EXPERIMENTAL PROCEDURES

Two hot rolled Ni-based superalloy GH3535 plates were welded together using pulsed current TIG semi-automatic welding. The welding stick material was also Ni-based superalloy GH3535. The chemical composition of the Ni-based superalloy GH3535 is listed in Table 1. The welded GH3535

was etched and examined using a metallographic microscope. The microstructure of the welded GH3535 is shown in Fig. 1. Some carbides (black) are distributed along the rolling direction in the PM (Fig. 1b). The microstructure of the WZ is mainly composed of small dendritic crystals (Fig. 1c). To produce the samples of the PM, the WZ and the HAZ for electrochemical experiments, each zone was masked with marking pen during metallographic examination and then cut into specimens by an electric spark cutting machine. All the samples were ground down using 1000 grit SiC paper, cleaned with distilled water and then dried. A Fe-Cr wire was spot welded to one end of the specimens for electrical connection. The sample was sealed in an alumina tube with high-temperature cement, with a length of 10 mm exposed. The cement was dried at room temperature for 24 h and then further solidified at 300 ^{o}C for 2 h. The exposed surfaces of samples were polished again with 1000 grit SiC paper, rinsed, and dried prior to testing.

The electrochemical tests, which included open circuit potentials, potentiodynamic polarization and galvanic corrosion measurements were conducted with a Princeton Applied Research PARSTAT 2273 potentiostat/Galvanostat system in a closed stainless steel chamber under the protection of a circulating high-purity Ar, as reported in Ref. [9]. Potentiodynamic polarization was undertaken at a scan rate of 20 mV· min^{-1}, using a conventional three-electrode system with a Pt electrode as the reference electrode and a graphite plate as the counter electrode. In the galvanic corrosion experiments, galvanic couple PM/WZ was selected. The galvanic potential (E_g) and current (I_g) of the couples were simultaneously recorded.

Table 1. Chemical composition of the Ni-based alloy GH3535 (expressed in terms of weight percent).

C	Mo	Cr	Fe	Mn	Si	Al	W	Ti
0.015	17.1	7.03	4.03	0.77	0.59	0.03	0.02	<0.01

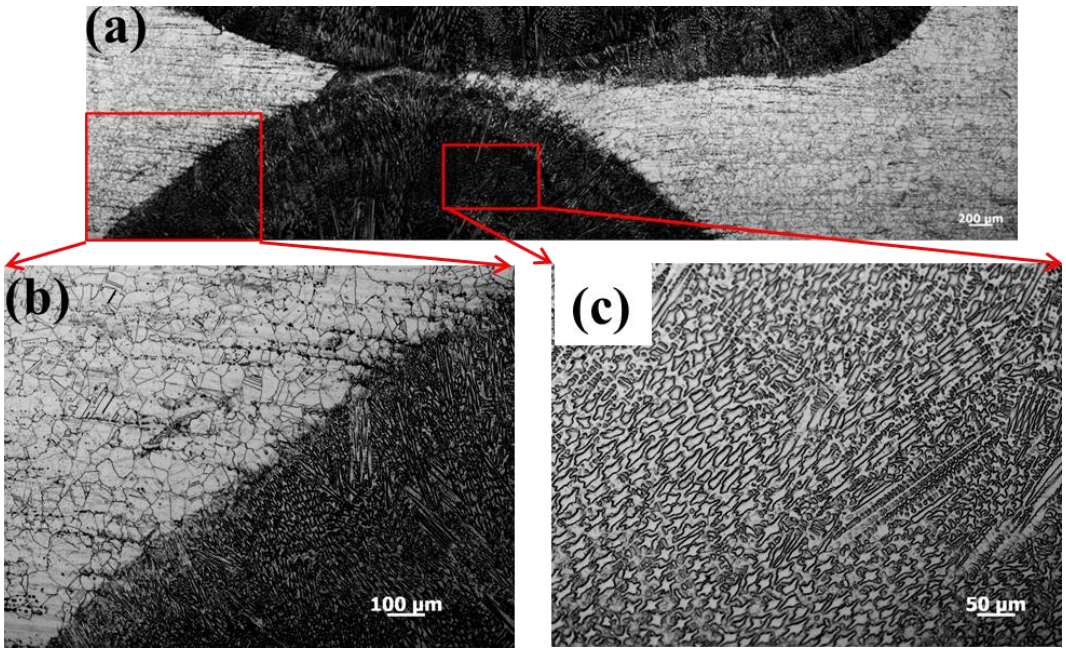

Figure 1. Microstructures of the welded GH3535: (a) the entire microstructure and (b) and (c): magnified images for the heat-affected zone (HAZ) and the weld zone (WZ).

A ternary eutectic mixture of 46.5LiF-11.5NaF-42KF (mole percent) was used for the corrosion study. After drying the LiF, NaF and KF, a mixture of (Li,Na,K)F with a mass of 178.6 g was placed into a graphite crucible. The salt mixture was further dried at 200 ^{o}C in the reaction chamber under vacuum, and then under the protection of Ar for 20 h before the furnace was heated to the experimental temperatures of 700 ^{o}C

After galvanic corrosion, the corroded samples covered with the remaining salts were mounted in epoxy resin and then their metallurgical sections were prepared using kerosene as coolant for grinding and polishing, with an attempt to examine the corroded metal/salt interface. Scanning electron microscopy (SEM) coupled with an energy dispersive X-ray microanalysis (EDX) was used to characterize the corroded samples.

3. RESULTS AND DISCUSSION

3.1 Open circuit potential measurements

Fig. 2 shows the change in the open circuit potential as a function of exposure time for different regions of the welded GH3535 in molten (Li,Na,K)F at 700 ^{o}C. The open circuit potential for the PM decreases gradually to -220 mV vs. Pt in the initial 20 min, and then shifts slowly to -200 mV vs. Pt. The open circuit potential for the HAZ is about -220 mV vs. Pt, with a little fluctuation in the entire immersion. The open circuit potential for the WZ is very negative during the initial stage at -275 mV vs. Pt, and then shifts positively to -210 mV vs. Pt, with a small fluctuation. It is clear that the WZ exhibits the most negative corrosion potential, then the PM and HAZ. The difference of the corrosion potential of the welded GH3535 probably leads to the galvanic corrosion.

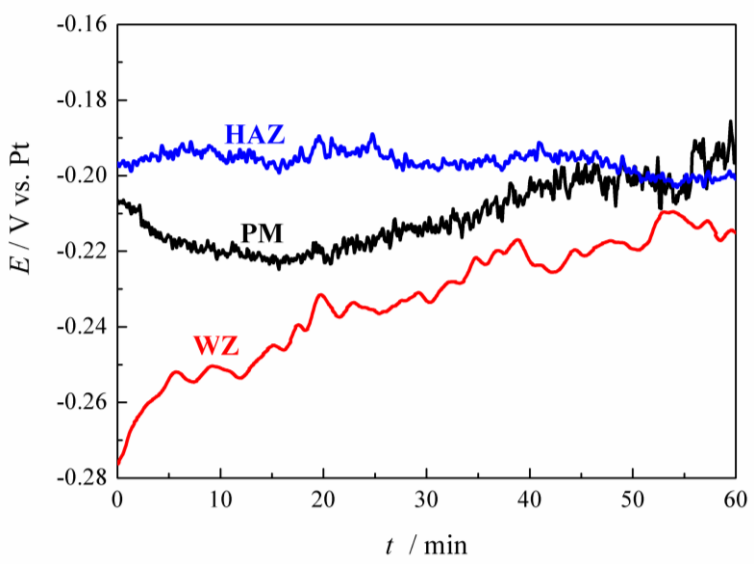

Figure 2. Open circuit potential curves for the PM, HAZ and WZ of the welded GH3535 in a eutectic (Li,Na,K)F melt at 700 ^{o}C in a pure Ar atmosphere.

3.2 Potentiodynamic polarization measurements

Fig. 3 shows the potentiodynamic polarization curves for different regions of the welded GH3535 in a eutectic (Li,Na,K)F melt at 700 ^{o}C in a pure Ar atmosphere. The results reveal that the PM, WZ and HAZ are in active states at the corrosion potential. The kinetic parameters for different regions of the welded GH3535 in molten (Li,Na,K)F at 700 ^{o}C are obtained using the Tafel extrapolation method with the results shown in Table 2. The corrosion current densities, I_{corr}, of the PM, HAZ and WZ are calculated to be approximately 106, 110 and 134 μA·cm^{-2}. The corrosion current density and the cathodic and anodic Tafel slopes of the PM and HAZ is in the same level, which indicating that the electrochemical behavior of the PM and HAZ in molten (Li,Na,K)F is similar. This result indicates that the corrosion resistance of the PM and HAZ in molten (Li,Na,K)F is better than that of the WZ.

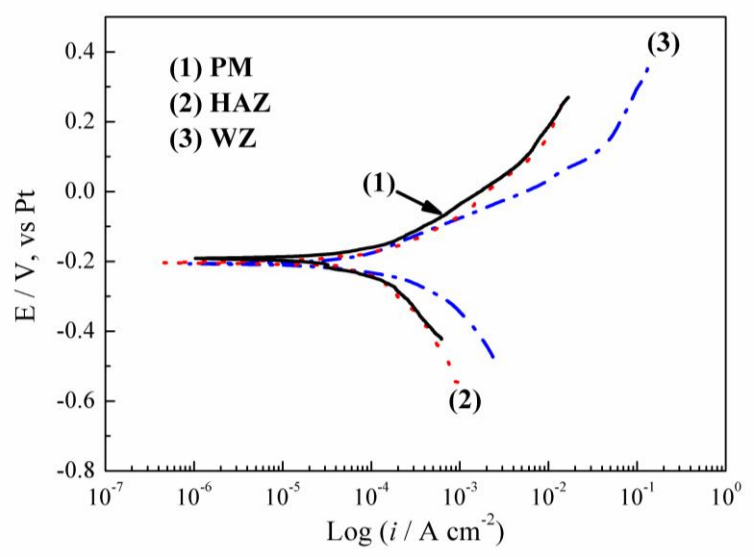

Figure 3. Potentiodynamic polarization curves for the PM, HAZ and WZ of the welded GH3535 in a eutectic (Li,Na,K)F melt at 700 ^{o}C in a pure Ar atmosphere.

Table 2. Fitting results of potentiodynamic curves for the PM, HAZ and WZ of the welded GH3535.

Samples	b_a (mV·dec^{-1})	b_c (mV·dec^{-1})	I_{corr} (μA·cm^{-2})	E_{corr} (mV vs. Pt)
PM	150.0	-319.0	106	-190
HAZ	155.0	-296.9	110	-195
WZ	98.9	-206.8	134	-200

3.3 Galvanic corrosion measurements

In view of the similar electrochemical behavior of the HAZ and PM, the galvanic corrosion

behavior of the PM/WZ couple is investigated. The time dependence of the galvanic potential and galvanic current density for the GH3535 PM/WZ couple at 700 ^{o}C in molten (Li,Na,K)F in a pure Ar atmosphere is shown in Fig. 4. Based on the above corrosion potential results, it can be inferred that the WZ acts as the anode during the galvanic corrosion process. The value of E_g for the galvanic couple goes through obvious fluctuations during the initial 40 min and then shifts negatively to about -200 mV vs. Pt. The value of I_g for the galvanic couple decreases drastically from 160 μA·cm^{-2} to 58.5 μA·cm^{-2} over the initial 10 min and then experiences a small fluctuation.

The average values of E_g and I_g are calculated using the integral method, as shown in Table 3. According to the relationship between the anodic dissolution current density (I_{corr}) and galvanic current density (I_g) [9] and the experimental results of the galvanic corrosion, the galvanic effect (γ) is calculated and listed in Table 3. It is seen that the value of γ is larger than 1, suggesting that the corrosion of the WZ sample is accelerated. The value of γ is much smaller than that for couples of different metals in molten (Li,Na,K)F at 700 ^{o}C reprted by Wang [9].

During the galvanic corrosion, the contact area ratio between the anode and the cathode plays an important role. According to the relationship between γ and the contact area ratio [9], the galvanic effect is proportional to the contact area ratio between the cathode and the anode. In the present study, the contact area ration between the PM and the WZ is 1. However, in actual environment, the area of the WZ is much smaller than the area of the PM, implying that the corrosion of the WZ becomes much more serious.

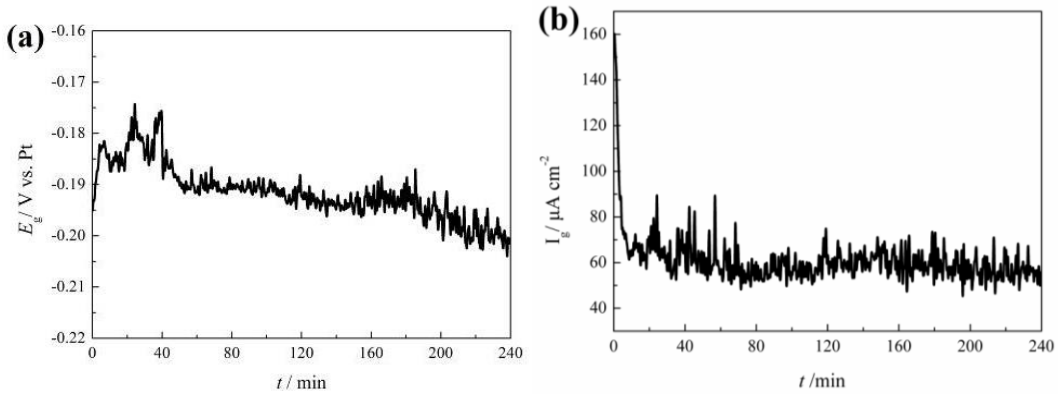

Figure 4. Time dependence of the galvanic potential (a) and galvanic current density (b) for the GH3535 PM/WZ couple at 700 ^{o}C in molten (Li,Na,K)F in a pure Ar atmosphere.

Table 3. Galavanic corrosion parameters for the GH3535 base/welding zone couple at 700 ^{o}C in molten (Li,Na,K)F in a pure Ar atmosphere.

Couple	$\overline{I_g}$ (μA/cm^2)	$\overline{E_g}$ (mV vs. Pt)	E_{corr} (mV vs. Pt)	I_a (μA/cm^2)	I_{corr} (μA/cm^2)	γ
PM/WZ	60.8	-190	-200	468	134	3.49

3.4 Characterization of the galvanically corroded samples

To examine the corroded material/salt mixture interface, the cross sections of the corroded

samples covered with the remaining salts were prepared for SEM observations. Fig. 5 presents the cross-sectional morphologies of the GH3535 WZ/PM couple corroded at 700 ^{o}C in molten (Li,Na,K)F under pure Ar for 4 h. The GH3535 PM and WZ are severely corroded through the non-uniform dissolution into the melt. Fe/Cr-depleted zones with depths of about 70 and 60 μm for the WZ and PM are observed due to the selective dissolution of Fe and Cr in molten (Li,Na,K)F. The depletion of Fe and Cr are similar to the results reported by Hou and Li [20, 21]. However, the Fe/Cr-depleted zones is deeper than those reported by Hou [20], which may be related to the amount of moisture impurities that are present.

In the present experiment, the main driving force for the corrosion of the PM and WZ is the electromotive potential difference and the residual moisture in molten (Li,Na,K)F. The residual moisture attacks the samples mainly through reacting with the fluorides to generate gaseous HF, which then dissolves into the melt and selectively reacts with the Fe and Cr in the samples. Coupled with the potential difference induced by the galvanic effect, the corrosion of the WZ sample experiences more severe corrosion than the the PM sample.

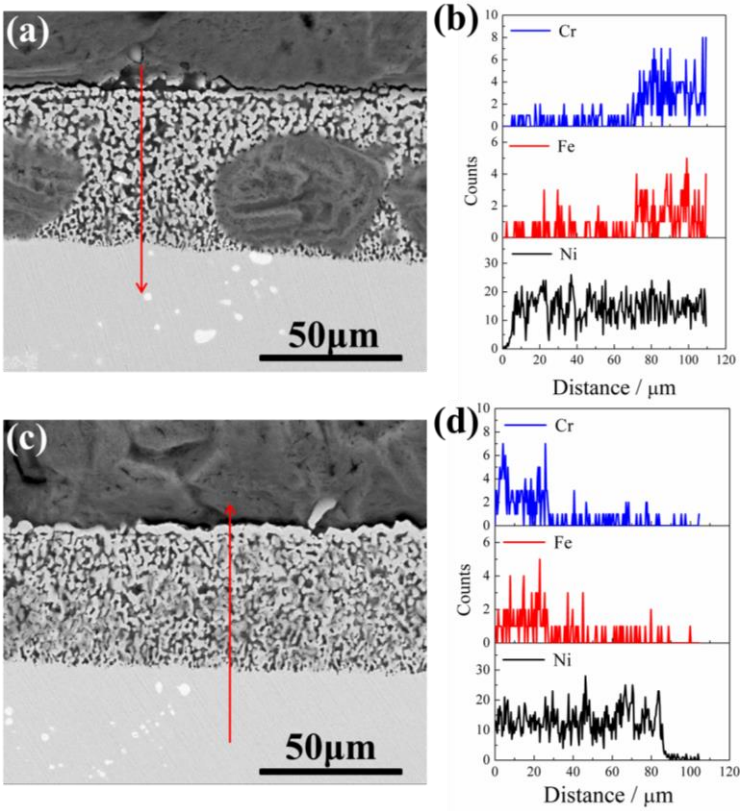

Figure 5. Cross-sectional morphologies and EDX analysis results of the GH3535 WZ ((a) and (b))/PM ((c) and (d)) couple corroded at 700 ^{o}C in molten (Li,Na,K)F in a pure Ar atmosphere for 4 h

4. CONCLUSIONS

In present study, the HAZ and PM of welded GH3535 show similar electrochemical behavior. Among the different zones of the welded GH3535, the corrosion current density for the WZ is the largest at about 134 μA·cm^{-2}. There exist potential differences among different zones of the welded

GH3535, especially for the weld zone and the parent material. When the weld zone of GH3535 is coupled with the parent material, galvanic corrosion occurs, with a galvanic corrosion effect of 3.49. The weld zone for the WZ/PM couple acts as the anode during the galvanic corrosion process, and the dissolution of Fe and Cr from the anode weld zone is promoted.

ACKNOWLEDGEMENTS
This project is supported by the Bagui scholars program of Guangxi autonomous region in 2016, the Academician Workstation Building Project of Guangxi Zhuang Autonomous Region Scientific and Technological Department [Grant No. [2014] 91], and National Natural Science Foundation of China [Grant No. 51271190].

References

1. S. Qiu, D. Zhang, G. Su, W. Tian, *Atom. Energ. Sci. Technol.*, 43(2009)64.
2. B. Zohuri, P. McDaniel, *Switzerland* (2015).
3. M. Kondo, T. Nagasaka, A. Sagara, N. Noda, T. Muroga, Q. Xu, M. Nagura, A. Suzuki and T. Terai, *J. Nucl. Mater.*, 386 (2009) 685.
4. H. Yamanishi and A. Sagara, *Annual Report of National Institute for Fusion Sci.*, (2000)177.
5. R.W. Moir, H.F. Shaw, A. Caro, L. Kaufman, J.F. Latkowski, J. Powers and P.E.A. Turchi, *Fusion Sci. Technol.*, 56 (2009) 632.
6. X. Ding, H. Sun, G. Yu, X. Zhou, *J. Chin. Soc. Corr. Pro.*, 35 (2015) 543.
7. K. Fukumoto, R. Fujimura, M. Yamawaki, Y. Arita, *J. Nucl. Sci. Technol.*, 52 (2015) 1323.
8. H. Wang, Q. Feng, Z. Wang, H. Zhou, Y. Kan, J. Hu, S. Dong, *J. Nucl. Mater.*, 487 (2017) 43.
9. Y. Wang, H. Liu, C. Zeng, *J. Fluorine Chem.*, 165 (2014) 1.
10. M. Seregin, A. Parshin, A.Y. Kuznetsov, L. Ponomarev, S. Mel'nikov, A. Mikhalichenko, A. Rzheutskii, R. Manuilov, *Ridiochem.*, 53 (2011) 491.
11. H. Zhu, R. Holmes, T. Hanley, J. Davis, K. Short, L. Edwards, *Corros. Sci.* 91 (2015) 1.
12. A. Pfennig, B. Fedelich, *Corros. Sci.*, 50 (2008) 2484.
13. M. Hofmeister, L. Klein, H. Miran, R. Rettig, S. Virtanen, R. F. Singer, *Corros. Sci.* 90 (2015) 46.
14. Y.L. Wang, Q. Wang, H.J. Liu, C.L. Zeng, *Corros. Sci.*, 109 (2016) 43.
15. W. Xue, X.Yang, J. Qiu, H. Liu, B. Zhao, H. Xia, X. Zhou, P. Huai, H. Liu, J. Wang, *Corros. Sci.*, 114 (2017) 96.
16. S. Delpech, C. Cabet, C. Slim, G.S. Picard, *Mater. Today*, 13(2010)34.
17. L.C. Olson, J.W. Ambrosek, K. Sridharan, M.H. Anderson, T.R. Allen, *J. Fluorine Chem.*, 130 (2009) 67.
18. M.S. Sohal, M.A. Ebner, P. Sabharwall, P. Sharpe, *INL/EXT-10-18297*, (2010).
19. J. Qiu, Y. Zou, G. Yu, H. Liu, Y. Jia, Z. Li, P. Huai, X. Zhou, H. Xu, *J. Fluorine Chem.*, 168 (2014) 69.
20. J. Hou, G. Yu, C. Zeng, H. Ai, R. Xie, Y. Chen, X. Zhou, L. Xie, J. Wang, *J. Fluorine Chem.*, 191 (2016) 110.
21. X. Li, S. He, X. Zhou, P. Huai, Z. Li, A. Li, X. Yu, *J. Nucl. Mater.*, 464 (2015) 342.